Laboratory Investigation (2019) 99:1107–1116
https://doi.org/10.1038/s41374-019-0253-6

ARTICLE

Lipoprotein modulation of proteinuric renal injury

Yohei Tsuchida[1] · Jianyong Zhong[1,2] · Tadashi Otsuka[1] · Anna Dikalova[3] · Ira Pastan[4] · G. M. Anantharamaiah[5] · MacRae F. Linton[3] · Patricia G. Yancey[3] · T. Alp Ikizler[3] · Agnes B. Fogo[1,2,3] · Haichun Yang[1,2] · Valentina Kon[1]

Received: 8 November 2018 / Revised: 8 February 2019 / Accepted: 4 March 2019 / Published online: 24 April 2019

Abstract

High-density lipoprotein (HDL) and its main protein, apolipoprotein AI (apoAI), have established benefits in various cells, but whether these cytoprotective effects of HDL pertain to renal cells is unclear. We investigated the in vitro consequences of exposing damaged podocytes to normal apoAI, HDL, and apoAI mimetic (L-4F), and the in vivo effects of L-4F on kidney and atherosclerotic injury in a podocyte-specific injury model of proteinuria. In vitro, primary mouse podocytes were injured by puromycin aminonucleoside (PAN). Cellular viability, migration, production of reactive oxygen species (ROS), apoptosis, and the underlying signaling pathway were assessed. In vivo, we used a proteinuric model, Nphs1-hCD25 transgenic (NEP25^{+}) mice, which express human CD25 on podocytes. Podocyte injury was induced by using immunotoxin (LMB2) and generated a proteinuric atherosclerosis model, NEP25^{+}:apoE$^{-/-}$ mice, was generated by mating apoE-deficient (apoE$^{-/-}$) mice with NEP25^{+} mice. Animals received L-4F or control vehicle. Renal function, podocyte injury, and atherosclerosis were assessed. PAN reduced podocyte viability, migration, and increased ROS production, all significantly lessened by apoAI, HDL, and L-4F. L-4F attenuated podocyte apoptosis and diminished PAN-induced inactivation of Janus family protein kinase-2/signal transducers and activators of transcription 3. In NEP25^{+} mice, L-4F significantly lessened overall proteinuria, and preserved podocyte expression of synaptopodin and cell density. Proteinuric NEP25^{+}:apoE$^{-/-}$ mice had more atherosclerosis than non-proteinuric apoE$^{-/-}$ mice, and these lesions were significantly decreased by L-4F. Normal human apoAI, HDL, and apoAI mimetic protect against podocyte damage. ApoAI mimetic provides in vivo beneficial effects on podocytes that culminate in reduced albuminuria and atherosclerosis. The results suggest supplemental apoAI/apoAI mimetic may be a novel candidate to lessen podocyte damage and its complications.

Introduction

Although chronic kidney disease (CKD) increases the risk for cardiovascular disease (CVD) and CVD potentiates CKD, the pathways linking these disorders and interventions that lessen the reciprocal potentiation of these diseases remain to be elucidated [1–4]. Hyperlipidemia, specifically elevated low-density lipoprotein cholesterol, is an essential mechanism underlying atherosclerotic CVD and is the central therapeutic target in CVD. The role of hyperlipidemia and the effects of lipid-lowering therapies on CKD are controversial [5, 6].

High-density lipoprotein (HDL) and its main protein, apolipoprotein AI (apoAI), have well-documented beneficial effects on various cell types by increasing cellular cholesterol efflux, and reducing oxidative stress, inflammation, and cellular apoptosis [7, 8]. The capacity of apoAI/HDL to affect cellular functionality is now considered a better parameter to gauge their benefits in CVD. This is relevant to CKD since renal disease causes apoAI/HDL to become dysfunctional, losing many vasoprotective effects while acquiring noxious properties that propel the pathophysiological pathways underlying CVD [9, 10]. Indeed, recent strategies targeting lipoprotein functionality, including supplementation with normal apoAI/HDL,

✉ Valentina Kon
Valentina.Kon@vanderbilt.edu

1 Departments of Pediatrics, Vanderbilt University Medical Center, Nashville, TN, USA

2 Departments of Pathology, Microbiology and Immunology, Vanderbilt University Medical Center, Nashville, TN, USA

3 Departments of Medicine, Vanderbilt University Medical Center, Nashville, TN, USA

4 Laboratory of Molecular Biology, Center for Cancer Research, NCI, NIH, Bethesda, MD, USA

5 Department of Medicine, University of Alabama, Birmingham, AL, USA

have supplanted HDL-raising interventions to reduce CVD [11, 12]. Currently, there is little understanding about the effects of normal or dysfunctional apoAI/HDL on progressive CKD, although impaired HDL functionality has been linked to progressive CKD [13]. Glomerular membrane selectivity limits the passage of large lipoproteins; however, the relatively small HDL and the even smaller constituent particles of HDL have been documented in the urine [14, 15]. At 28 kDa, apoAI is less than half the size of albumin (66.5 kDa) and is thus predicted to cross the glomerular filtration barrier. Renal injuries that involve disruption in the glomerular capillaries are expected to allow filtration of more dysfunctional lipoproteins to interact with renal parenchymal cells beyond the barrier. This scenario is relevant because albuminuria reflects disruption of the filtration barrier and is a very strong independent risk factor for CKD as well as CVD [16, 17].

To evaluate how apoAI/HDL affects podocytes and proteinuric renal and atherosclerotic injuries, we studied the effects of apoAI, HDL, and apoAI mimetic in normal and damaged podocytes and examined the impact of these interventions on renal injury and atherosclerosis in a podocyte-specific proteinuric mouse model.

Materials and methods

Animals and systemic parameters

In vivo studies were done using a well-established model of proteinuria, Nphs1-hCD25 transgenic ($NEP25^+$) mice. $NEP25^+$ mice express human CD25 on podocytes that can be selectively injured by injection of recombinant immunotoxin, anti-Tac (Fv)- PE38 (LMB2) that results in proteinuria [18, 19]. These animals were crossed with atherosclerosis-prone apoE-deficient mice ($apoE^{-/-}$) to generate $NEP25^+$:$apoE^{-/-}$ mice to assess the effects of proteinuria on atherosclerosis. Fourteen-week-old $NEP25^+$:$apoE^{-/-}$ mice were injected with LMB2 (1 ng/g BW, i.v.) and compared to identically treated littermate controls ($NEP25^-$:$apoE^{-/-}$). The mice were fed a normal chow diet and killed 4 weeks later. In studies assessing the effects of apoAI mimetic, L-4F, $NEP25^+$, and $NEP25^+$:$apoE^{-/-}$ were randomized to groups that received either L-4F (100 µg i.p. 3× a week for 2 weeks in $NEP25^+$ mice and for 4 weeks in $NEP25^+$:$apoE^{-/-}$ mice) or saline vehicle [20, 21]. The animal protocol was approved by Vanderbilt University Medical Center Institutional Animal Care and Use Committee in accordance with the National Institutes of Health guidelines.

Body weight (BW) was assessed, and spot urine samples were obtained. Urinary apoAI was measured by Elisa (MyBiosource, SanDiego, CA, USA). Albuminuria was measured as spot urine albumin-to-creatinine ratio (ACR) using Albuwell M (Exocell, Philadelphia, PA, USA) and the QuantiChrom™ Creatinine Assay Kit (Bio Assay Systems, Hayward, CA, USA), respectively. Systemic blood pressure (BP) was measured in conscious trained animals by using a tail cuff at sacrifice using the BP-2000 SERIES II Blood Pressure Analysis System™ (Visitech Systems Inc., Apex, NC, USA). Blood was collected at sacrifice to measure the levels of serum total cholesterol and triglyceride by high-performance liquid chromatography (HPLC) and blood urea nitrogen (BUN) by the QuantiChrom™ Urea Assay Kit (Bio Assay Systems).

Histological assessments

To assess atherosclerosis, mice were killed under phenobarbital anesthesia and perfused with PBS through the left ventricle. The entire aorta, from the aortic valves to the iliac bifurcation, was dissected and the en face preparations opened longitudinally, pinned flat, and stained with Sudan IV (Sigma, St. Louis, MO, USA). The atherosclerotic lesions were compared by computerized analysis with lesions expressed as a percentage of the total vascular surface [22, 23]. The operator was blinded to the group assignment.

The kidneys were fixed in 4% paraformaldehyde and embedded in paraffin. For collagen IV staining, tissues were digested with 0.1% trypsin (Sigma) at 37 °C for 25 min. Citrate buffer antigen retrieval was done by microwaving for 15 min, cooling for 20 min, and then incubating with H_2O_2 in methanol (1:100) for 15 min. Synaptopodin was stained using the M.O.M. Immunodetection kit (Vector Laboratories, Burlingame, CA, USA). For Wilms' tumor 1 (WT1) and collagen IV staining, sections were blocked with 2.5% normal horse serum (Vector Laboratories) for 1 h, incubated with primary antibodies overnight, and then exposed to monoclonal anti-rat synaptopodin (Progen, Heidelberg, Germany), anti-mouse WT1 (Abcam, Cambridge, UK), anti-mouse collagen IV (EMD Millipore, Burlington, MA, USA), or anti-mouse apoAI (Abcam). To quantify expression of each staining, all kidney samples were processed and sectioned at the same time. Thirty glomeruli, excluding tangential sections, were photographed with AxioCam MRc5 (Carl Zeiss, Oberkochen, Germany) under the same conditions. The ratio of synaptopodin or collagen IV-positive area to glomerular tuft area and the density of WT1-positive cells in glomerular tuft area for each glomerulus were determined by Image J software (National Institutes of Health). The average ratio was determined for each mouse.

In vitro assessment of cell viability, migration, and superoxide production

Primary podocytes were isolated from 5- to 7-week-old wild-type mouse using a modified method of iron beads perfusion (Invitrogen, Carlsbad, CA, USA); collagenase A dissociation (Roche Applied Science, Penzberg, Germany); and sieving as previously described (BD Falcon, Bedford, MA, USA) [24, 25]. In brief, mouse kidneys perfused with iron beads were minced and then digested in collagenase A (1.5 mg/ml) at 37 °C for 30 min. After sieving, bead-containing glomeruli were collected by a magnetic particle concentrator, washed of all tubular structures and suspended in DMEM/Ham's F12 containing 0.2-μm-filtered 3T3-L1 supernatant, 5% FBS, ITS solution, and 100 U/ml penicillin-streptomycin. The glomeruli were then plated onto collagen type I precoated dishes and incubated at 37 °C in room air with 5% CO_2. After 3 days, cell colonies began to sprout. The cells showed epithelial morphology with a polyhedral shape and were characterized as podocytes by WT1 and synaptopodin staining. Only cells less than the fourth passage were used in in vitro experiments.

Cells were incubated for 24 h with or without puromycin aminonucleoside (PAN) (100 μg/ml) and apoAI (10 μg/ml), HDL (50u g/ml), or L-4F (50 μg/ml). HDL used in the current study was isolated from participants of a previously completed study of normal controls approved by the Institutional Review Board at Vanderbilt University Medical Center (#121293). HDL was isolated by the well-established method of density gradient ultracentrifugation after adjustment with potassium bromide [26], then frozen at −80 °C and thawed only once, which we and others have shown as having minimal effect on functionality [10, 27, 28]. ApoAI was purchased from EMD Millipore. The podocyte cell viability assay was performed using the XTT cell viability kit (Cell Signaling Technology, Danvers, MA, USA). The same design was used in the wound-healing assay to assess migration. The migration rate between 0 and 11 h after scratch was calculated as percent change using the formula [100 × (Pre-length − Post-length)/Pre-length].

Migration experiments were performed in triplicate wells. Podocyte production of superoxide was measured as cellular formation of the superoxide-specific product of dihydroethidium, 2-hydroxyethidium, using HPLC analysis. The experimental design followed that described for variability and migration studies [29].

Immunoblot analyses were done in podocytes cultured in medium with/without PAN and L-4F for 24 h. Total protein was extracted by using an RIPA buffer containing EDTA, EGTA, phosphatase inhibitor, and protease inhibitor (Roche). Equal amounts of total proteins were separated by NuPAGE 4–12% Bis-Tris gel electrophoresis and electrophoretically transferred to nitrocellulose membranes by using an iBlot system (Invitrogen) blocked with 5% albumin from bovine serum (Sigma) in Tris-buffered saline containing 0.1% TWEEN 20 (TBS-T) and incubated with primary antibody for cleaved caspase-3 (1:500), p53 (1:1000), phosphorylated Janus family protein kinase-2 (JAK2) on tyrosine 1007/1008) (1:1000) and phosphorylated signal transducers and activators of transcription 3 (STAT3) on tyrosine 705 (1:1000) from Cell Signaling Technology or β-actin (1:5000) from Sigma at 4 °C overnight. After washing, horseradish peroxidase-labeled IgG secondary antibodies (1:3000 for rabbit and 1:5000 for mouse in 5% powdered nonfat milk/TBS-T, Promega, Madison, WI, USA) were added and incubated at room temperature for 1 h. Protein bands were visualized by Western Lightning Plus-ECL (Perkin Elmer, Waltham, MA, USA). Abundance of protein expression, shown as a specific band, was analyzed by Image J software, normalized by loading control (β-actin).

Statistical analysis

Results are expressed as means ± SEM. Statistical difference was assessed by a single-factor analysis of variance (ANOVA) followed by unpaired *t*-test with corrections for multiple comparisons as appropriate. $P < 0.05$ was considered to be significant.

Results

Podocyte injury causes proteinuria and potentiates atherosclerosis

ACR was significantly higher in NEP25^{+}:apoE$^{-/-}$ (generated by crossing the NEP25^{+} and atherosclerosis-prone apoE$^{-/-}$) than in NEP25^{-}:apoE$^{-/-}$ mice (Fig. 1a). ACR peaked at 7 days and remained elevated until sacrifice. Although BW, systemic BP, total cholesterol, triglycerides, and BUN were not different between the groups at the end of the study (Table 1), proteinuric animals had more extensive atherosclerotic lesions, with a threefold increase in the area covered by atherosclerotic plaques in proteinuric NEP25^{+}:apoE$^{-/-}$ mice than in non-proteinuric NEP25^{-}:apoE$^{-/-}$ mice (Fig. 1b).

Podocyte damage is lessened by normal ApoAI or HDL

We next evaluated how injured podocytes are affected by exposure to normal lipoproteins. For this purpose, we injured cultured podocytes by exposing them to PAN and assessed the effects of normal apoAI or HDL of normal

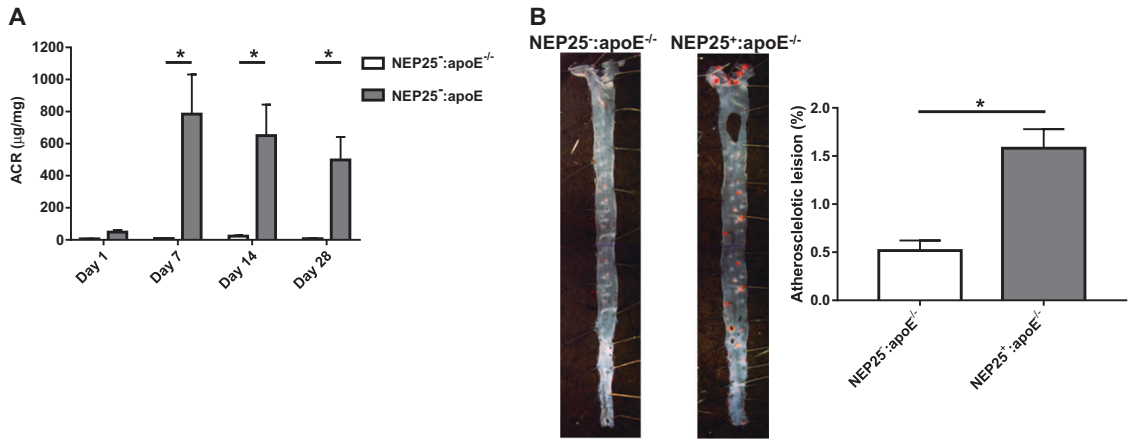

Fig. 1 Albuminuria and atherosclerosis in NEP25^{-}:apoE$^{-/-}$ and NEP25^{+}:apoE$^{-/-}$ mice. **a** Urine albumin-creatinine ratio (ACR) at 1, 7, 14, and 28 days after LMB2. **b** En face pinned-open aortas stained with Sudan IV. Graph shows the quantitative data of atherosclerosis in NEP25^{-}:apoE$^{-/-}$ and NEP25^{+}:apoE$^{-/-}$. Mean ± SEM, $n = 5$ in each group. *$P < 0.05$

Table 1 Systemic parameters in NEP25^{-}:apoE$^{-/-}$ versus NEP25^{+}:apoE$^{-/-}$

	NEP25^{-}:apoE$^{-/-}$	NEP25^{+}:apoE$^{-/-}$	*P* value
BW (g)	23.1 ± 1.2	23.4 ± 1.0	NS
Systolic BP (mmHg)	109 ± 10	110 ± 11	NS
Total cholesterol (mg/dl)	318.5 ± 57.1	358.1 ± 66.4	NS
Triglycerides (mg/dl)	71.9 ± 13.7	84.4 ± 4.8	NS
BUN (mg/dl)	31.3 ± 9.9	33.2 ± 4.5	NS

controls without renal disease. PAN caused a significant reduction in podocyte viability. This effect was significantly abated by podocyte exposure to normal human apoAI and also exposure to HDL (Fig. 2a). Compared with untreated cells, PAN also decreased podocyte migration. Both apoAI and HDL blunted this decreased migration (Fig. 2b). To investigate the effects of apoAI/HDL on the podocyte oxidant response, we measured superoxide as a measure of reactive oxygen species (ROS) production in podocytes exposed to PAN and apoAI, HDL. PAN significantly increased podocyte oxidative stress level. However, cellular exposure to apoAI or HDL lessened this response (Fig. 2c). Together, these data indicate that normal apoAI or HDL can protect podocytes against injurious stimuli.

ApoAI mimetic, L-4F, improves damaged podocytes and proteinuric renal injury

The increasing appreciation that kidneys participate in metabolism of apoAI/HDL prompted us to evaluate how proteinuria affects renal lipoprotein and how lipoproteins affect podocyte injury. Figure 3a shows apoAI immunostaining that illustrates more glomerular immunostaining in proteinuric NEP25^{+} mice compared to non-proteinuric NEP25^{-} mice and also juxtaposition of apoAI with podocytes in kidneys of NEP25^{+} proteinuric mice (Fig. 3a). This observation is complemented by data showing a striking increase in urinary apoAI in NEP25^{+} mice compared to non-proteinuric NEP25^{-} controls where apoAI was non-detectable (Fig. 3b).

Since proteinuric disease increases urinary lipoproteins, we next examined whether supplementation with a synthetic apoAI mimetic, L-4F, would improve glomerular podocyte response in vitro. apoAI mimetics have previously been shown to reduce or repress atherosclerosis [30, 31] and lessen renal damage following sepsis, unilateral ureteral obstruction of subtotal nephrectomy and angiotensin infusion [32, 33]. We studied the effects of L-4F on podocytes damaged by PAN. L-4F added to PAN-injured podocytes significantly improved cellular viability (Fig. 4a), migration (Fig. 4b), and lessened ROS production (Fig. 4c). To evaluate apoptosis and the underlying signaling pathway, cleaved caspase-3, p53, and phosphorylated JAK2/STAT3 were assessed. PAN significantly increased cleaved caspase-3. Cellular exposure to L-4F significantly lessened this response (Fig. 4d). p53 showed the same pattern, increasing with PAN-injury that abated in response to L-4F (Fig. 4e). PAN significantly decreased phosphorylated JAK2 that was attenuated by L-4F (Fig. 4f). Phosphorylated STAT3 followed the same response, decreasing after PAN, improved with exposure to L-4F (Fig. 4g).

To determine whether the beneficial effects of apoAI mimetic on damaged podocytes in vitro could be seen in vivo, we treated NEP25^{+} proteinuric mice with L-4F. L-4F administration did not affect the BW, systolic BP, lipid profile, or BUN (Table 2). As shown in Fig. 5, 1 week after administration of LMB2, there was a dramatic increase in albuminuria, which was similar in treated and untreated

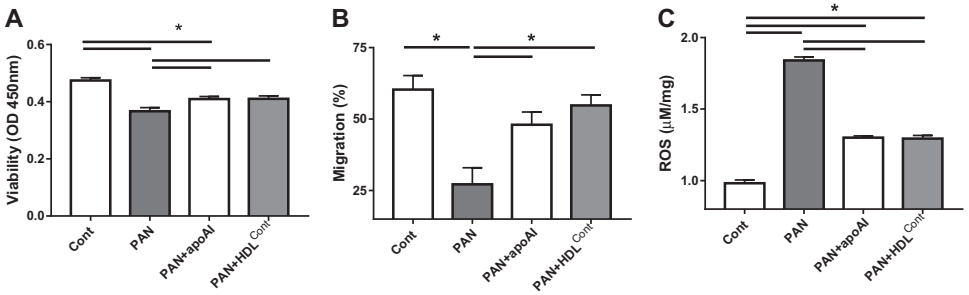

Fig. 2 Effects of normal apolipoprotein AI (apoAI) and high-density lipoprotein (HDL) from normal subjects on cultured podocytes injured by puromycin aminonucleoside (PAN). **a** Cell viability was assessed by the colorimetric assay, **b** migration was assessed by scratch test, and **c** cellular production of reactive oxygen species (ROS) was measured by high-performance liquid chromatography. Mean ± SEM, $n = 6$ in each group. $^*P < 0.05$

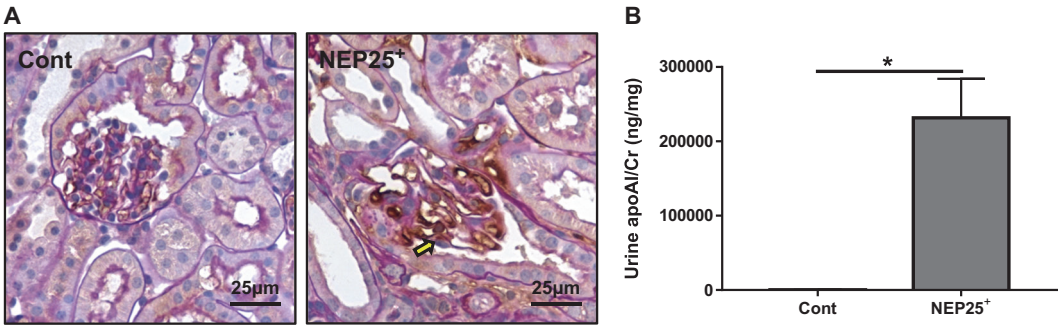

Fig. 3 **a** Representative micrograph illustrating juxtaposition of apolipoprotein AI (apoAI) with podocytes in glomeruli of $NEP25^-$ and $NEP25^+$ mice. **b** Urinary apoAI in $NEP25^-$ and $NEP25^+$ mice 14 days after LMB2. Mean ± SEM, $n = 8$ in each group. $^*P < 0.05$

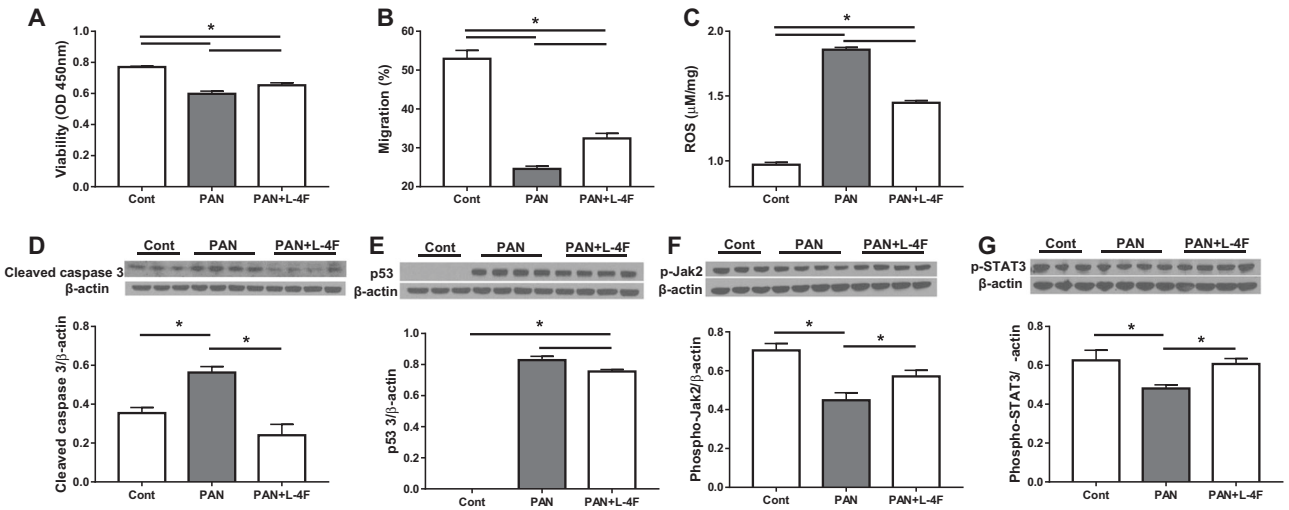

Fig. 4 Effects of the apolipoprotein AI (apoAI) mimetic, L-4F, on podocytes injured by puromycin aminonucleoside (PAN). **a** Cell viability was assessed by the colorimetric assay, **b** migration by scratch test, and **c** cellular production of reactive oxygen species (ROS) measured by high-performance liquid chromatography. Specific immunoblotting bands for **d** cleaved caspase-3, **e** p53, **f** phosphorylated Janus family protein kinase-2 (p-JAK2) (tyrosine 1007/1008), and **g** phosphorylated signal transducers and activators of transcription 3 (p-STAT3) (tyrosine 705) were analyzed by image J software and quantitated as the average ratio of specific bands/β-actin bands. Mean ± SEM, $n = 6$ in each group. $^*P < 0.01$

mice. Notably, the reduction in proteinuria by the second week was significantly greater in mice treated with L-4F (Fig. 5a). To determine if this reduction in albuminuria is linked to less podocyte injury, we examined the kidneys of $NEP25^+$ proteinuric mice with or without L-4F treatment. The podocyte differentiation marker, synaptopodin, was

significantly preserved in kidneys of NEP25^{+} proteinuric mice treated with L-4F versus untreated mice (Fig. 5b). Complementing these findings, podocyte density quantified by staining of WT1, a marker of mature podocytes, was preserved in the treated group (Fig. 5c). L-4F treatment also significantly lessened mesangial matrix expansion by expression of collagen IV compared to vehicle-treated proteinuric mice (Fig. 5d).

ApoAI mimetic, L-4-F, improves proteinuria-driven atherosclerosis

Our initial study showed that albuminuric NEP25^{+}:apoE$^{-/-}$ mice have more atherosclerosis than NEP25^{-}:apoE$^{-/-}$ mice (Fig. 1). Therefore, we examined if supplementation with apoAI mimetic can affect this augmented atherosclerosis induced by podocyte damage. For this purpose, we determined the extent of atherosclerosis in NEP25^{+}:apoE$^{-/-}$ mice treated with L-4F. We chose a 4-week treatment course because the dose of LMB2 used causes albuminuria over this time frame and because it is sufficiently long to demonstrate progression of atherosclerosis. Administration of L-4F for 4 weeks did not affect the BW, systolic BP, lipid profile, or BUN (Table 3). As in NEP25^{+} mice, the apoAI mimetic reduced albuminuria in the NEP25^{+}:apoE$^{-/-}$ mice (Fig. 6a). Atherosclerosis was significantly reduced in these mice with L-4F treatment compared to mice without L-4F treatment as assessed in en face aortas by Sudan IV staining (Fig. 6b).

Table 2 Systemic arameters in Nep25^{+} ± L-4F

	NEP25^{+} + Vehicle	NEP25^{+} + L-4F	*P* value
BW (g)	23.5 ± 1.1	25.4 ± 1.6	NS
Systolic BP (mmHg)	107 ± 11	100 ± 6	NS
Total cholesterol (mg/dl)	77.8 ± 5.4	73.6 ± 4.7	NS
Triglycerides (mg/dl)	20.0 ± 5.6	26.4 ± 3.8	NS
BUN (mg/dl)	39.9 ± 3.1	35.8 ± 2.0	NS

Discussion

Our study shows that podocyte injury in vitro can be ameliorated by normal apoAI/HDL. ApoAI mimetic also protected podocytes against injury through mechanisms involving reduced apoptosis and maintenance of the activated JAK2/STAT3 pathway. In vivo, this podocyte-injury-induced proteinuria amplified atherogenesis in NEP25^{+}:apoE$^{-/-}$ mice compared to non-proteinuric NEP25^{-}:apoE$^{-/-}$ mice, an effect not dependent on changes in BP, renal function, or lipid profile. ApoAI mimetic preserved glomerular synaptopodin expression and podocyte density, together with reduction of albuminuria in NEP25^{+} mice. It also significantly blunted atherosclerosis in proteinuric NEP25^{+}:apoE$^{-/-}$ mice. These data indicate that normal apoAI/HDL as well as apoAI mimetic can lessen podocyte

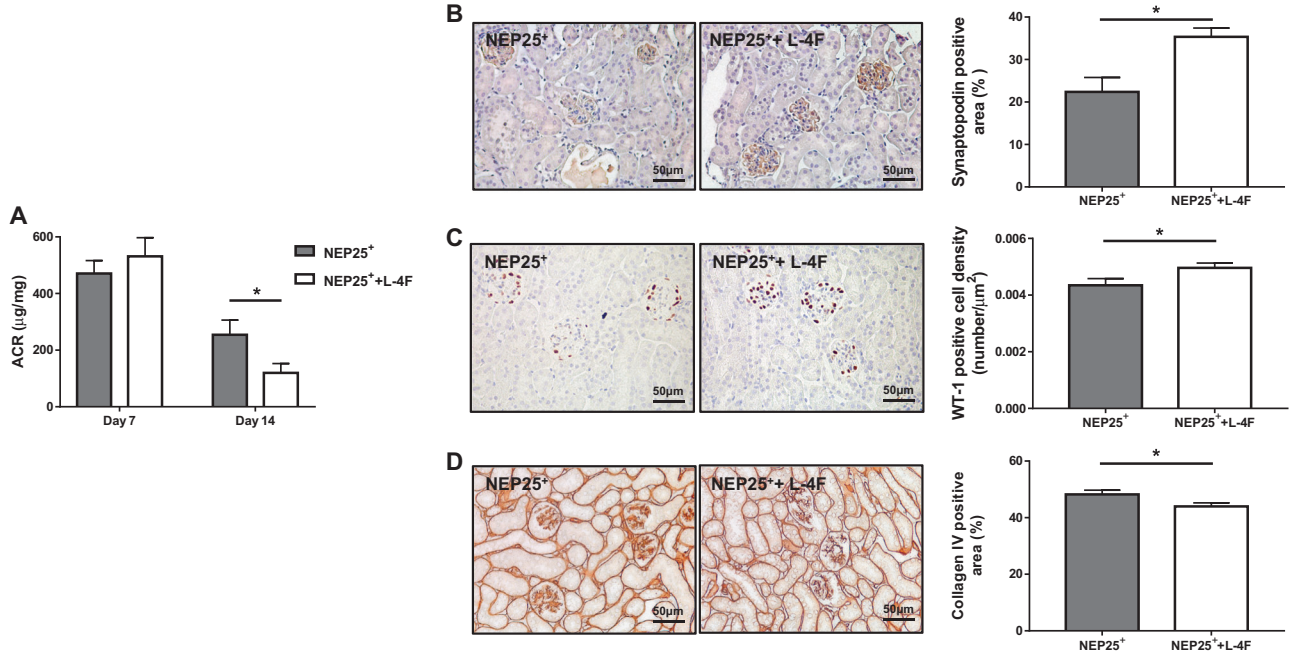

Fig. 5 Effects of the apolipoprotein AI (apoAI) mimetic, L-4F, on albuminuria and glomerular structure of NEP25^{+} mice. **a** Urine albumin-creatinine ratio (ACR) at 7 and 14 days after LMB2. **b** Immunostaining was quantified as the ratio of synaptopodin-stained area/glomerular tuft area, **c** Wilms' tumor 1 (WT1)-stained cell number/glomerular tuft area. **d** Ratio of collagen IV-stained area/glomerular tuft area. Magnification ×400. Mean ± SEM, $n = 8$ in each group. *$P < 0.05$

Table 3 Systemic parameters in Nep25^{+}/ApoE$^{-/-}$ with or without L-4F treatment

	NEP25^{+}:apoE$^{-/-}$ + Vehicle	NEP25^{+}:apoE$^{-/-}$ + L-4F	*P* value
BW (g)	22.4 ± 2.1	21.6 ± 2.0	NS
Systolic BP (mmHg)	112 ± 12	106 ± 4	NS
Total cholesterol (mg/dl)	335.4 ± 47.9	391.5 ± 75.9	NS
Triglycerides (mg/dl)	76.3 ± 18.1	102.1 ± 18.4	NS
BUN (mg/dl)	44.0 ± 7.2	48.1 ± 8.5	NS

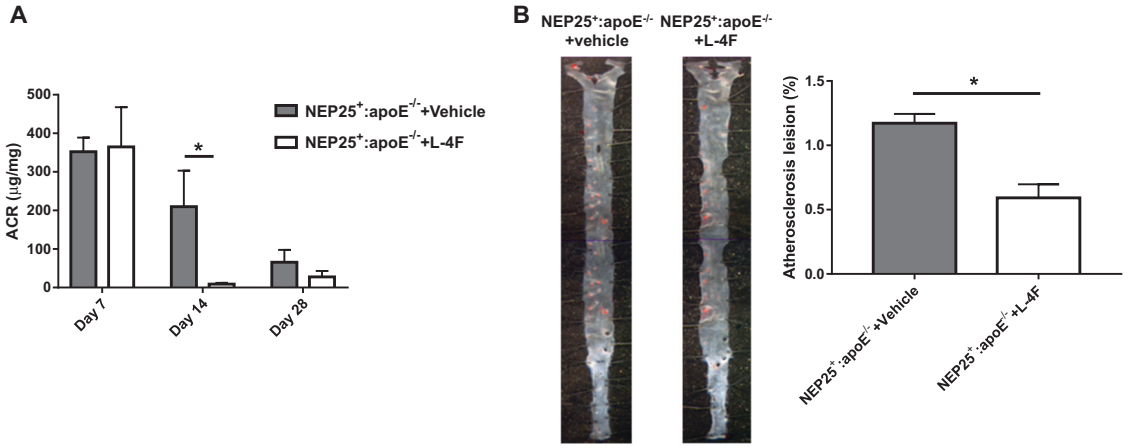

Fig. 6 Effects of the apolipoprotein AI (apoAI) mimetic, L-4F, on albuminuria and atherosclerosis in NEP25^{+}:apoE$^{-/-}$ mice. **a** ApoAI mimetic, L-4F, lessened albuminuria and atherosclerosis in NEP25^{+} albuminuric mice. Urine albumin-creatinine ratio (ACR) at 7, 14, and 28 days after LMB2. **b** Representative pictures of en face pinned-open aortas stained with Sudan IV. Graph shows the quantitative data of atherosclerosis in NEP25^{+}:apoE$^{-/-}$ with or without L-4F treatment. Mean ± SEM, $n = 8$ in each group. $^{*}P < 0.05$

injury, reduce albuminuric kidney damage and abate atherosclerosis.

Filtration of the potentially anomalous lipoproteins may be particularly relevant in albuminuric settings since albuminuria per se amplifies atherosclerotic CVD and is a very strong risk factor of cardiovascular mortality and progressive CKD [16]. The current study shows that even in the absence of changes in systemic cholesterol, triglycerides, or BP, proteinuric animals develop more extensive atherosclerosis than non-proteinuric mice. Albuminuria has been put forth as reflecting a generalized endothelial cell dysfunction. In our model, proteinuria is unlikely to reflect systemic endothelial dysfunction as it is created by specifically damaging the podocytes. Thus, renal specific damage can rapidly amplify atherosclerotic vasculopathy and does not necessarily depend on systemic endothelial dysfunction or hyperlipidemia, which often accompanies proteinuria, especially severe proteinuria. Nonetheless, it is possible that proteinuric kidney disease alters apoAI/HDL function, which can contribute to vasculopathy. Previous studies have noted that, even in the absence of reduced glomerular filtration rate, proteinuria can alter levels, distribution in particle size and composition of the HDL particles [14, 34–36].

In addition to the classical link between apoAI/HDL, macrophage foam cells, and atherosclerotic CVD, there is an increasing recognition that apoAI/HDL interacts with and provides beneficial effects to many different types of cells, in many organ systems; including endothelial cells, cardiomyocytes, and adipocytes [8, 37]. Relatively little is understood about whether apoAI/HDL interacts with and benefits renal parenchymal cells. In part, this is due to limitations imposed by the glomerular filtration barrier, which restricts passage of most plasma proteins and large molecules. However, disruption in the glomerular filter that characterizes proteinuric kidney injury predicts increased passage of a greater number of particles, including apoAI/HDL [38]. Our study in NEP25^{+} mice shows colocalization of apoAI with podocytes, which suggests passage of this plasma protein across the glomerular filtration barrier. The observation is supported by elevated levels of urinary apoAI in NEP25^{+} proteinuric mice compared to control mice (Fig. 3). Normally, filtered apoAI is reabsorbed by tubular epithelial cells expressing receptors (cubilin/megalin) [39]. In addition, kidneys express transporters for apolipoproteins and HDL, including ATP-binding cassette transporter-A1 and scavenger receptor-BI, which we recently found to have an important role in binding, trafficking, or salvage of filtered apoAI [38]. Deficiency or disruption of the transporters or receptor affects tubular handling of apoAI [39, 40]. Thus, increased urinary apoAI in our NEP25^{+} model likely reflects disruption of the

glomerular filtration barrier, together with some degree of tubular damage.

Because of the limited volume of mouse HDL samples, we tested our hypothesis that normal apoAI or HDL can protect damaged podocytes, using human apoAI/HDL. We exposed PAN-injured podocytes to normal apoAI or HDL from subjects with normal kidney function. Our data show that normal apoAI as well as HDL from normal subjects improves cellular viability, increases migration, and reduces production of ROS in PAN-injured podocytes (Fig. 2). These observations complement previous reports that podocytes exposed to sera of albuminuric diabetics with nephropathy had greater impairment in cholesterol efflux than podocytes exposed to sera of nonalbuminuric diabetic patients, despite similar lipid profiles and duration of diabetes [41]. In the same study, cyclodextrin treatment to mend lipoprotein functionality improved efflux in cultured podocytes, preserved podocyte function, and lessened albuminuria. Similar benefits of cyclodextrin were recently observed in NFATc1-dependent podocyte injury as well as nonmetabolic disorders, including experimental Alport syndrome and adriamycin-induced model of focal segmental glomerulosclerosis [42, 43]. Interestingly, a prospective study in renal transplant recipient found that, while HDL efflux capacity did not predict cardiovascular or all-cause mortality, a strong inverse association between graft failure and HDL efflux capacity was observed [13]. Together, these data support the concept that normal apoAI/HDL modulate renal cell function and impact pathways involved in progressive renal damage.

The shift in the therapeutic goal of raising HDL-C levels to enhancing HDL function prompted us to evaluate the therapeutic implications of supplementing with an apoAI mimetic, L-4F, previously reported to lessen inflammation and oxidation [44–46]. Our results show that L-4F significantly improved viability of PAN-injured podocytes, increased migration and lessened ROS production (Fig. 4). These beneficial effects of apoAI mimetic were directionally similar to the benefits observed in injured podocytes exposed to native apoAI or HDL of normal non-CKD subjects (Fig. 2). In complementary studies we showed that, at least in part, the beneficial effects involve reduction in apoptosis, as reflected by the reduction of cleaved caspase-3 and p53 expression in PAN-injured podocytes (Fig. 4). ApoAI and apoAI mimetic have previously been reported to prevent apoptosis by activation of the JAK2/STAT3 pathway [47]. The current study also shows podocyte activation of JAK2/STAT3, implicated in apoptosis, which can be inhibited by the apoAI mimetic. Activation of the JAK2/STAT3 signaling pathway reduces apoptosis in various cells, including adipocytes and cancer cells [48–51]. In podocytes, activation of the JAK2 pathway by the erythropoiesis-stimulating protein, darbepoetin alfa, reduces podocyte apoptosis and proteinuria [52]. In cardiac microvascular endothelial cells, activation of the JAK2/STAT3 signaling pathway also reduces apoptosis induced by cellular oxidative stress [53]. Antioxidant intervention can ameliorate podocyte apoptosis [54, 55]. Overall, these reports fit with our observations that the antioxidative capacity of apoAI mimetic lessens podocyte apoptosis through activation of the JAK2/STAT3 signaling pathway.

To determine the in vivo consequences of apoAI mimetic, we directly infused L-4F into albuminuric mice. L-4F preserved podocyte structure and density with significantly less albuminuria than untreated mice (Fig. 5). L-4F also significantly reduced the extent of atherosclerosis in NEP25^{+}:apoE$^{-/-}$ mice compared to untreated NEP25^{+}:apoE$^{-/-}$ mice (Fig. 6). This antiatherogenic effect of apoAI mimetic may reflect their antioxidative capacity. Indeed, oxidative stress induced by higher ROS production and lower antioxidant defenses is increasingly recognized as a critical cardiovascular risk factor in the CKD setting [54]. Our observations that normal apoAI, HDL, and apoAI mimetic can all lessen ROS in injured podocytes but also benefit CVD are consistent with the suggestion that local ROS production drives systemic stress [56, 57]. It is also possible that apoAI mimetic lessens ROS throughout the body. Interestingly, immune modulation by apoAI mimetics appears to be a pivotal pathway for the beneficial effects observed in a variety of diseases, including sepsis, cancer, asthma and progressive fibrosis [58–61]. Regardless of mechanism, reduction of kidney disease per se may be the key mechanism for reduction in atherosclerosis in that setting.

In conclusion, our study shows that proteinuric kidney disease increases atherosclerosis. Normal apoAI/HDL and apoAI mimetic have protective effects on damaged podocytes. Direct infusion of apoAI mimetic significantly lessens glomerular damage, proteinuria, and atherosclerosis. Based on these results, we suggest that using supplemental apoAI/apoAI mimetic may be a novel intervention to lessen podocyte damage, and the resulting proteinuria and atherosclerosis.

Acknowledgements The authors acknowledge the expert technical assistance of Cathy Xu and Youmin Zhang.

Compliance with ethical standards

Conflict of interest This work was supported by National Heart, Lung, and Blood Institute grant P01HL116263 and GM115367 and DK108836. This research was supported in part by the Intramural Research Program of the NIH, National Cancer Institute, Center for Cancer Research.

References

1. Go AS, Chertow GM, Fan D, McCulloch CE, Hsu CY. Chronic kidney disease and the risks of death, cardiovascular events, and hospitalization. N Engl J Med. 2004;351:1296–305.
2. Briasoulis A, Bakris GL. Chronic kidney disease as a coronary artery disease risk equivalent. Curr Cardiol Rep. 2013;15:340.
3. Liu M, Li XC, Lu L, Cao Y, Sun RR, Chen S, et al. Cardiovascular disease and its relationship with chronic kidney disease. Eur Rev Med Pharmacol Sci. 2014;18:2918–26.
4. Said S, Hernandez GT. The link between chronic kidney disease and cardiovascular disease. J Nephropathol. 2014;3:99–104.
5. Tonelli M, Wanner C.Kidney Disease: Improving Global Outcomes Lipid Guideline Development Work Group M Lipid management in chronic kidney disease: synopsis of the kidney disease: improving global outcomes 2013 clinical practice guideline. Ann Intern Med. 2014;160:182
6. Massy ZA, de Zeeuw D. LDL cholesterol in CKD--to treat or not to treat? Kidney Int. 2013;84:451–6.
7. deGoma EM, Rader DJ. High-density lipoprotein particle number: a better measure to quantify high-density lipoprotein? J Am Coll Cardiol. 2012;60:517–20.
8. Umemoto T, Han CY, Mitra P, Averill MM, Tang C, Goodspeed L, et al. Apolipoprotein AI and high-density lipoprotein have anti-inflammatory effects on adipocytes via cholesterol transporters: ATP-binding cassette A-1, ATP-binding cassette G-1, and scavenger receptor B-1. Circ Res. 2013;112:1345–54.
9. Rysz-Gorzynska M, Banach M. Subfractions of high-density lipoprotein (HDL) and dysfunctional HDL in chronic kidney disease patients. Arch Med Sci. 2016;12:844–9.
10. Yamamoto S, Yancey PG, Ikizler TA, Jerome WG, Kaseda R, Cox B, et al. Dysfunctional high-density lipoprotein in patients on chronic hemodialysis. J Am Coll Cardiol. 2012;60:2372–9.
11. Kingwell BA, Chapman MJ, Kontush A, Miller NE. HDL-targeted therapies: progress, failures and future. Nat Rev Drug Discov. 2014;13:445–64.
12. Tardif JC, Ballantyne CM, Barter P, Dasseux JL, Fayad ZA, Guertin MC, et al. Effects of the high-density lipoprotein mimetic agent CER-001 on coronary atherosclerosis in patients with acute coronary syndromes: a randomized trial. Eur Heart J. 2014;35: 3277–86.
13. Annema W, Dikkers A, de Boer JF, Dullaart RP, Sanders JS, Bakker SJ, et al. HDL cholesterol efflux predicts graft failure in renal transplant recipients. J Am Soc Nephrol. 2016;27:595–603.
14. Soto-Miranda E, Carreon-Torres E, Lorenzo K, Bazan-Salinas B, Garcia-Sanchez C, Franco M, et al. Shift of high-density lipoprotein size distribution toward large particles in patients with proteinuria. Clin Chim Acta. 2012;414:241–5.
15. Lopez-Olmos V, Carreon-Torres E, Luna-Luna M, Flores-Castillo C, Martinez-Ramirez M, Bautista-Perez R, et al. Increased HDL size and enhanced apo A-I catabolic rates are associated with doxorubicin-induced proteinuria in New Zealand white rabbits. Lipids. 2016;51:311–20.
16. Sarnak MJ, Astor BC. Implications of proteinuria: CKD progression and cardiovascular outcomes. Adv Chronic Kidney Dis. 2011;18:258–66.
17. Fung KY, Wang C, Nyegaard S, Heit B, Fairn GD, Lee WL. SR-BI mediated transcytosis of HDL in brain microvascular endothelial cells is independent of caveolin, clathrin, and PDZK1. Front Physiol. 2017;8:841.
18. Matsusaka T, Xin J, Niwa S, Kobayashi K, Akatsuka A, Hashizume H, et al. Genetic engineering of glomerular sclerosis in the mouse via control of onset and severity of podocyte-specific injury. J Am Soc Nephrol. 2005;16:1013–23.
19. Matsusaka T, Sandgren E, Shintani A, Kon V, Pastan I, Fogo AB, et al. Podocyte injury damages other podocytes. J Am Soc Nephrol. 2011;22:1275–85.
20. Navab M, Reddy ST, Anantharamaiah GM, Imaizumi S, Hough G, Hama S, et al. Intestine may be a major site of action for the apoA-I mimetic peptide 4F whether administered subcutaneously or orally. J Lipid Res. 2011;52:1200–10.
21. Rudolf M, Mir Mohi Sefat A, Miura Y, Tura A, Raasch W, Ranjbar M, et al. ApoA-I Mimetic Peptide 4F Reduces Age-Related Lipid Deposition in Murine Bruch's Membrane and Causes Its Structural Remodeling. Curr Eye Res. 2018;43:135–46.
22. Ayabe N, Babaev VR, Tang Y, Tanizawa T, Fogo AB, Linton MF, et al. Transiently heightened angiotensin II has distinct effects on atherosclerosis and aneurysm formation in hyperlipidemic mice. Atherosclerosis. 2006;184:312–21.
23. Fazio S, Major AS, Swift LL, Gleaves LA, Accad M, Linton MF, et al. Increased atherosclerosis in LDL receptor-null mice lacking ACAT1 in macrophages. J Clin Invest. 2001;107:163–71.
24. Ma J, Matsusaka T, Yang HC, Zhong J, Takagi N, Fogo AB, et al. Induction of podocyte-derived VEGF ameliorates podocyte injury and subsequent abnormal glomerular development caused by puromycin aminonucleoside. Pediatric Res. 2011;70:83–9.
25. Takemoto M, Asker N, Gerhardt H, Lundkvist A, Johansson BR, Saito Y, et al. A new method for large scale isolation of kidney glomeruli from mice. Am J Pathol. 2002;161:799–805.
26. Jerome WG, Cox BE, Griffin EE, Ullery JC. Lysosomal cholesterol accumulation inhibits subsequent hydrolysis of lipoprotein cholesteryl ester. Microsc Microanal. 2008;14:138–49.
27. Rohatgi A, Khera A, Berry JD, Givens EG, Ayers CR, Wedin KE, et al. HDL cholesterol efflux capacity and incident cardiovascular events. N Engl J Med. 2014;371:2383–93.
28. Kekulawala JR, Murphy A, D'Souza W, Wai C, Chin-Dusting J, Kingwell B, et al. Impact of freezing on high-density lipoprotein functionality. Anal Biochem. 2008;379:213–5.
29. Dikalova AE, Bikineyeva AT, Budzyn K, Nazarewicz RR, McCann L, Lewis W, et al. Therapeutic targeting of mitochondrial superoxide in hypertension. Circ Res. 2010;107:106–16.
30. Navab M, Anantharamaiah GM, Hama S, Hough G, Reddy ST, Frank JS, et al. D-4F and statins synergize to render HDL anti-inflammatory in mice and monkeys and cause lesion regression in old apolipoprotein E-null mice. Arterioscler Thromb Vasc Biol. 2005;25:1426–32.
31. Navab M, Anantharamaiah GM, Hama S, Garber DW, Chaddha M, Hough G, et al. Oral administration of an Apo A-I mimetic peptide synthesized from D-amino acids dramatically reduces atherosclerosis in mice independent of plasma cholesterol. Circulation. 2002;105:290–2.
32. Moreira RS, Irigoyen M, Sanches TR, Volpini RA, Camara NO, Malheiros DM, et al. Apolipoprotein A-I mimetic peptide 4F attenuates kidney injury, heart injury, and endothelial dysfunction in sepsis. Am J Physiol Regul Integr Comp Physiol. 2014;307: R514–24.
33. Souza AC, Bocharov AV, Baranova IN, Vishnyakova TG, Huang YG, Wilkins KJ, et al. Antagonism of scavenger receptor CD36 by 5A peptide prevents chronic kidney disease progression in mice independent of blood pressure regulation. Kidney Int. 2016;89:809–22.
34. Shearer GC, Newman JW, Hammock BD, Kaysen GA. Graded effects of proteinuria on HDL structure in nephrotic rats. J Am Soc Nephrol. 2005;16:1309–19.
35. Bulum T, Kolaric B, Duvnjak L. Lower levels of total HDL and HDL3 cholesterol are associated with albuminuria in normoalbuminuric Type 1 diabetic patients. J Endocrinol Investig. 2013;36:574–8.

36. Godfrey L, Yamada-Fowler N, Smith J, Thornalley PJ, Rabbani N. Arginine-directed glycation and decreased HDL plasma concentration and functionality. Nutr Diabetes. 2014;4:e134.
37. Speer T, Zewinger S, Fliser D. Uraemic dyslipidaemia revisited: role of high-density lipoprotein. Nephrol Dial Transplant. 2013; 28:2456–63.
38. Zhong J, Yang H, Kon V. Pediatric Nephrol 2018. https://doi.org/10.1007/s00467-018-4104-2.
39. Nielsen R, Christensen EI, Birn H. Megalin and cubilin in proximal tubule protein reabsorption: from experimental models to human disease. Kidney Int. 2016;89:58–67.
40. Graversen JH, Castro G, Kandoussi A, Nielsen H, Christensen EI, Norden A, et al. A pivotal role of the human kidney in catabolism of HDL protein components apolipoprotein A-I and A-IV but not of A-II. Lipids. 2008;43:467–70.
41. Merscher-Gomez S, Guzman J, Pedigo CE, Lehto M, Aguillon-Prada R, Mendez A, et al. Cyclodextrin protects podocytes in diabetic kidney disease. Diabetes. 2013;62:3817–27.
42. Pedigo CE, Ducasa GM, Leclercq F, Sloan A, Mitrofanova A, Hashmi T, et al. Local TNF causes NFATc1-dependent cholesterol-mediated podocyte injury. J Clin Investig. 2016;126:3336–50.
43. Mitrofanova A, Molina J, Varona Santos J, Guzman J, Morales XA, Ducasa GM, et al. Hydroxypropyl-beta-cyclodextrin protects from kidney disease in experimental Alport syndrome and focal segmental glomerulosclerosis. Kidney Int. 2018;94:1151–115.
44. Imaizumi S, Navab M, Morgantini C, Charles-Schoeman C, Su F, Gao F, et al. Dysfunctional high-density lipoprotein and the potential of apolipoprotein A-1 mimetic peptides to normalize the composition and function of lipoproteins. Circ J. 2011;75:1533–8.
45. Getz GS, Wool GD, Reardon CA. Biological properties of apolipoprotein A-I mimetic peptides. Curr Atheroscler Rep. 2010; 12:96–104.
46. Rosenbaum MA, Chaudhuri P, Abelson B, Cross BN, Graham LM. Apolipoprotein A-I mimetic peptide reverses impaired arterial healing after injury by reducing oxidative stress. Atherosclerosis. 2015;241:709–15.
47. Liu Y, Tang C. Regulation of ABCA1 functions by signaling pathways. Biochim Biophys Acta. 2011;1821:522–9.
48. Liu Z, Gan L, Zhou Z, Jin W, Sun C. SOCS3 promotes inflammation and apoptosis via inhibiting JAK2/STAT3 signaling pathway in 3T3-L1 adipocyte. Immunobiology. 2015;220:947–53.
49. Zhang T, Jiang B, Zou ST, Liu F, Hua D. Overexpression of B7-H3 augments anti-apoptosis of colorectal cancer cells by Jak2-STAT3. World J Gastroenterol. 2015;21:1804–13.
50. Um HJ, Min KJ, Kim DE, Kwon TK. Withaferin A inhibits JAK/STAT3 signaling and induces apoptosis of human renal carcinoma Caki cells. Biochem Biophys Res Commun. 2012;427: 24–9.
51. Bill MA, Nicholas C, Mace TA, Etter JP, Li C, Schwartz EB, et al. Structurally modified curcumin analogs inhibit STAT3 phosphorylation and promote apoptosis of human renal cell carcinoma and melanoma cell lines. PLoS ONE. 2012;7: e40724.
52. Logar CM, Brinkkoetter PT, Krofft RD, Pippin JW, Shankland SJ. Darbepoetin alfa protects podocytes from apoptosis in vitro and in vivo. Kidney Int. 2007;72:489–98.
53. Zhao XB, Qin Y, Niu YL, Yang J. Matrine inhibits hypoxia/reoxygenation-induced apoptosis of cardiac microvascular endothelial cells in rats via the JAK2/STAT3 signaling pathway. Biomed Pharmacother. 2018;106:117–24.
54. Liu T, Chen XM, Sun JY, Jiang XS, Wu Y, Yang S, et al. Palmitic acid-induced podocyte apoptosis via the reactive oxygen species-dependent mitochondrial pathway. Kidney Blood Press Res. 2018;43:206–19.
55. Hua W, Huang HZ, Tan LT, Wan JM, Gui HB, Zhao L, et al. CD36 mediated fatty acid-induced podocyte apoptosis via oxidative stress. PLoS ONE. 2015;10:e0127507.
56. Hernandez-Rios P, Pussinen PJ, Vernal R, Hernandez M. Oxidative stress in the local and systemic events of apical periodontitis. Front Physiol. 2017;8:869.
57. Vaziri ND. Oxidative stress in uremia: nature, mechanisms, and potential consequences. Semin Nephrol. 2004;24:469–73.
58. Dai L, Datta G, Zhang Z, Gupta H, Patel R, Honavar J, et al. The apolipoprotein A-I mimetic peptide 4F prevents defects in vascular function in endotoxemic rats. J Lipid Res. 2010;51: 2695–705.
59. Zamanian-Daryoush M, Lindner D, Tallant TC, Wang Z, Buffa J, Klipfell E, et al. The cardioprotective protein apolipoprotein A1 promotes potent anti-tumorigenic effects. J Biol Chem. 2013;288: 21237–52.
60. Van Linthout S, Spillmann F, Riad A, Trimpert C, Lievens J, Meloni M, et al. Human apolipoprotein A-I gene transfer reduces the development of experimental diabetic cardiomyopathy. Circulation. 2008;117:1563–73.
61. Su F, Grijalva V, Navab K, Ganapathy E, Meriwether D, Imaizumi S, et al. HDL mimetics inhibit tumor development in both induced and spontaneous mouse models of colon cancer. Mol Cancer Ther. 2012;11:1311–9.